Electronic Supplementary Information for 'Ultrafast photoisomerisation of an isolated retinoid'

James N. Bull, Christopher W. West, Cate S. Anstöter, Gabriel da Silva, Evan J. Bieske, Jan R. R. Verlet

ATDs with collisional excitation in the ion source

Arrival time distributions (ATDs) for *trans*-RA$^-$ recorded with a low and high RF drive voltage applied to the source ion funnel are shown in Fig. S1. The 'off' ATD shows a single peak consistent with just the *trans* isomer. In contrast, a high RF drive voltage to the source ion funnel ('high' ATD) gives increased ion throughput but also induces violent collisions between ions and buffer gas molecules promoting statistical isomerisation to more compact isomers (although the ATD is still dominated by the *trans* isomer peak).

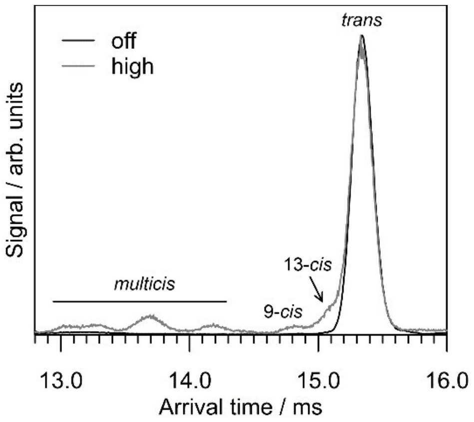

Fig. S1 – ATDs for *trans*-RA$^-$ in N_2 buffer gas with no ('off') or 'high' RF drive voltages applied to the source ion funnel.

Photoaction ATDs with different light fluences

Photoaction ATDs for *trans*-RA¯ in which the ions were intercepted with a 3.49 eV (355 nm) pulse of light immediately after their injection into the drift region are shown in Fig. 2(c) and 3(b) in the paper. The photoisomer ATD peaks were assigned to the 13-*cis* and 9-*cis* isomers by aligning ATD peak arrival times with those for pure samples of each isomer.

The photoaction ATDs recorded as part of the PISA spectroscopy procedure involved irradiating mobility-selected *trans*-RA¯ at the end of the first drift region (IMS1). Any photoisomers were separated in the second drift region (IMS2). Photoaction ATDs for *trans*-RA¯ in N_2 buffer gas at 3.49 eV with different light fluences are shown in Fig. S2. Note that the photoisomer ATD peaks appear at approximately half the arrival time of the corresponding isomers separated in the entire drift region (Fig. 2(c) in the paper). The photoaction ATD with light fluence 0.4 mJ cm^{-2} pulse^{-1} has two peaks, assigned to the 13-*cis* and 9-*cis* photoisomers. Increasing the light fluence to 1.0 mJ cm^{-2} pulse^{-1} resulted in signal at shorter arrival times, which is consistent with formation of *dicis* isomers formed through sequential isomerisations, e.g. *trans* → 13-*cis* → *dicis*. Light fluences of <0.4 mJ cm^{-2} pulse^{-1} gave <4% photoresponse across the photon energy range considered in this work.

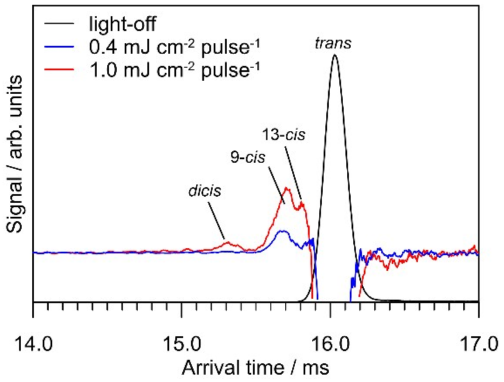

Fig. S2 – Photoaction ATDs (with ×20 scaling) for mobility-selected *trans*-RA¯ in N_2 buffer gas at the photon energy of 3.49 eV. PISA spectra in the paper were recorded with light fluence <0.4 mJ cm^{-2} pulse^{-1} to minimise sequential absorption processes. Note, the *trans*-RA¯ ATD peak is shifted in arrival time compared with the ATDs in Fig. 2 in the paper due to a different pressure of N_2 buffer gas (measurements performed on different days).

Solution absorption spectra

UV-Vis absorption spectra (Fig. S3) for *trans*, 13-*cis* and 9-*cis* isomers of retinoic acid dissolved in pure methanol and *trans* retinoic acid dissolved in methanol adjusted to pH > 11 using ammonia were recorded with a Varian CaryBio 50 spectrophotometer. The *trans* and 13-*cis* spectra both peak at 3.70 eV (335 nm). The peak of the 9-*cis* spectrum is blue-shifted by ≈0.10 eV and has increased absorption at higher photon energies. The absorption spectrum for *trans*-RA$^-$ in pH > 11 methanol is nearly identical to that for *trans* in neutral methanol.

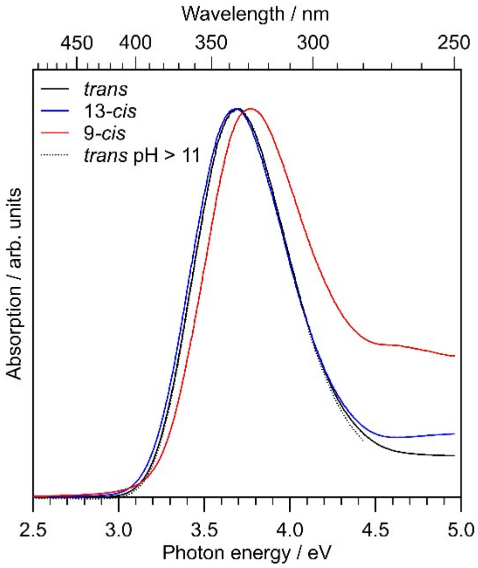

Fig. S3 – UV-Vis absorption spectra for the *trans*, 13-*cis* and 9-*cis* isomers of retinoic acid in pure methanol solution and *trans*-RA$^-$ in pH > 11 methanol. Each spectrum was acquired in a single, low intensity scan to minimise photoisomerisation by the spectrometer probe light.

RRKM rates for *cis*-RA$^-$→ *trans*-RA$^-$ isomerisation

RRKM theory rate constants, $k(E)$, for *trans*-RA$^-$ → single-*cis*-RA$^-$ transformations are discussed in the paper (Fig. 5). $k(E)$ values for the reverse single-*cis*-RA$^-$ → *trans*-RA$^-$ transformations are given in Fig. S4. Because the rates for isomerisation about odd-numbered double bonds are much lower than the collision rate in the drift region ($\approx 10^9$ s^{-1}), any 13-*cis*, 11-*cis* and 9-*cis* photoisomers formed through an ultrafast photoisomerisation process should be stabilised before they statistically revert to the lower energy *trans* isomer.

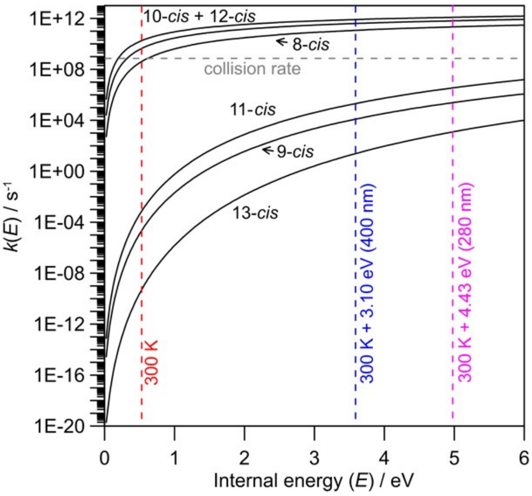

Fig. S4 – RRKM theory rates, k(E), for statistical isomerisation of *cis*-RA$^-$ isomers to *trans*-RA$^-$. Vertical lines correspond to the initial thermal energy of the ions at 298 K (red, 0.56 eV), plus the energy imparted by a 3.10 eV (400 nm, blue) and 4.43 eV (280 nm, violet) photon. Note the log scale for k(E).

3.10 + 1.55 eV time-resolved data for *trans*-RA^{-}

The time-resolved measurements reported in the paper used a 3.10 + 2.49 eV pump-probe scheme offering ≈70 fs cross-correlation. Time-resolved measurements were also performed with a 3.10 + 1.55 eV pump-probe scheme (Fig. S5), which offered slightly reduced pump-probe cross-correlation (≈50 fs) and improved characterisation of t_{A1} = 80 fs.

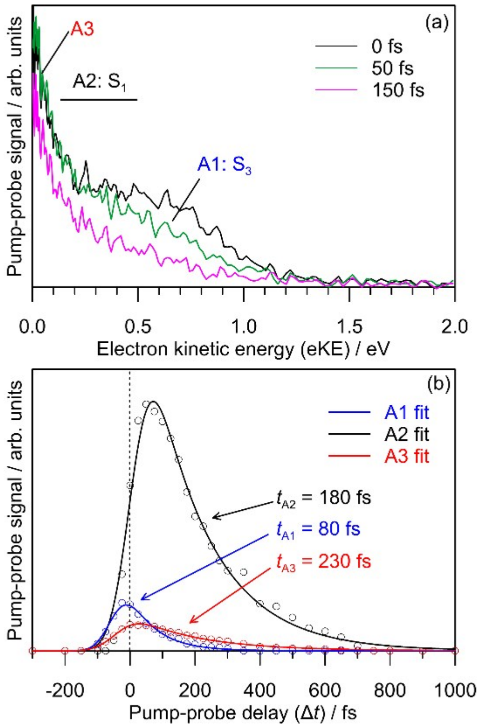

Fig. S5 – 3.10 + 1.55 eV time-resolved photoelectron data for *trans*-RA^{-}: (a) three example time-resolved spectra, and (b) contributions of each pump-probe feature. The fitted (Gaussian) cross correlation in (b) is 50±5 fs. A1 is assigned to $S_3(\pi\pi^*) \rightarrow S_1(\pi\pi^*)$ internal conversion, A2 to $S_1(\pi\pi^*) \rightarrow S_0$ internal conversion and concomitant isomerisation. A3 is tentatively assigned to detachment processes following $S_n \leftarrow S_1(\pi\pi^*)$ (n = 3-5) excitation induced by the probe. Errors in fitted timescales are ±10 fs.

Fitting procedure for time-resolved data

The time-resolved photoelectron spectra were obtained by subtracting a pump-only spectrum (i.e. $\Delta t = -500$ fs) from each pump-probe spectrum (i.e. $\Delta t \geq -200$ fs). Time-resolved spectra for 'rigid' molecules (defined as having little nuclear motion associated with the excited state dynamics) are conventionally interpreted in terms of static basis functions (eKE bands) that are fixed in eKE across all time-resolved spectra. However, isomerising anions have large changes in geometry and a varying energy difference between anionic and neutral potential energy surfaces with Δt, requiring interpretation with time-varying basis functions. Our fit model assumed the following three basis functions:

1. A static Gaussian function for the $S_3(\pi\pi^*)$ state population (feature A1).
2. A moving Gaussian function for the $S_1(\pi\pi^*)$ population (feature A2). The peak eKE position of this function was free to vary in a smooth decreasing manner with Δt (Fig. 7(c) in the paper shows a smooth <eKE> with Δt).
3. A static Boltzmann-like (thermionic emission) distribution for feature A3.

Both the 3.10 + 2.49 eV and 3.10 + 1.55 eV pump-probe data sets were simultaneous fit with the same model. Example pump-probe feature and total fits for the Δt = 50 and 300 fs time-resolved spectra recorded with the 2.49 eV probe are shown in Fig. S5.

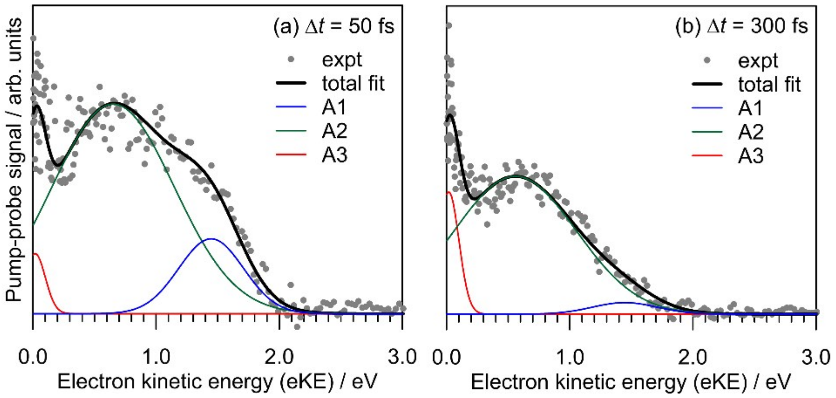

Fig. S5 – Example fits for the Δt = (a) 50 fs and (b) 300 fs time-resolved spectra with the 3.10 + 2.49 eV pump-probe scheme. A1 is assigned to $S_3(\pi\pi^*) \rightarrow S_1(\pi\pi^*)$ internal conversion, A2 is assigned to $S_1(\pi\pi^*) \rightarrow S_0$ internal conversion (and concomitant isomerisation), and A3 is tentatively assigned to $S_n \leftarrow S_1(\pi\pi^*)$ (n=2-5) excitation induced by the probe followed by internal conversion and autodetachment.

CASSCF natural orbitals

The CASSCF(16,13) reference wavefunction was comprised of the 13 natural orbitals shown below. The CASSCF(12,11) active space excluded orbitals 1 and 2. At the *trans*-RA$^-$ geometry, the $S_1(\pi\pi^*) \leftarrow S_0$ transition is dominated by 9 (LUMO) ← 7 (HOMO-1) orbital excitation, the $S_2(n\pi^*) \leftarrow S_0$ transition is dominated by 9 (HOMO) ← 6 (*n*) orbital excitation, and the $S_3(\pi\pi^*) \leftarrow S_0$ transition is dominated by 9 (LUMO) ← 8 (HOMO) orbital excitation. The $S_3(\pi\pi^*) \leftarrow S_0$ transition is analogous to the $S_2(\pi\pi^*) \leftarrow S_0$ (B_u^+) transition in *beta*-carotenes.

1 (*n*) 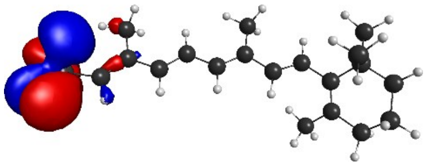	**2 (*n*)** 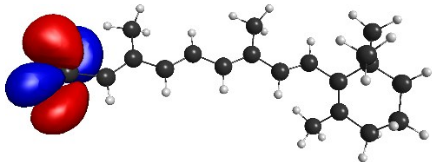
3 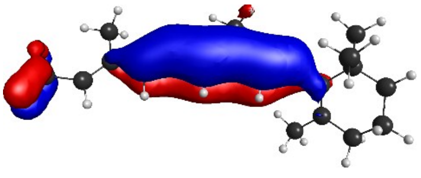	**4** 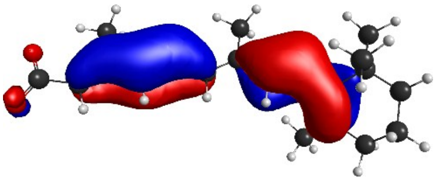
5 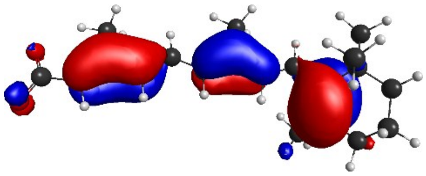	**6 (*n*)** 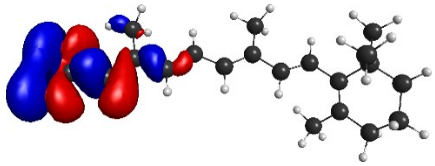
7 (HOMO-1) 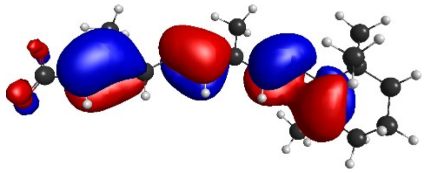	**8 (HOMO)** 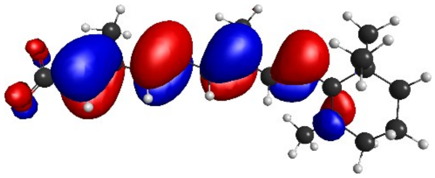
9 (LUMO) 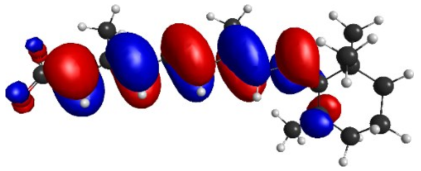	**10** 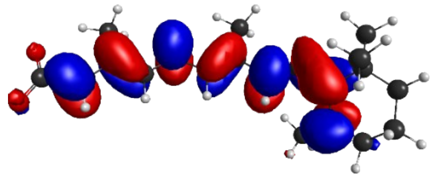
11 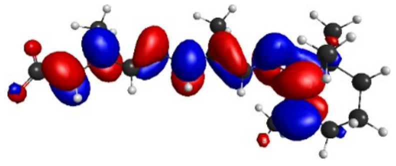	**12** 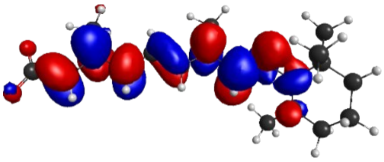
13 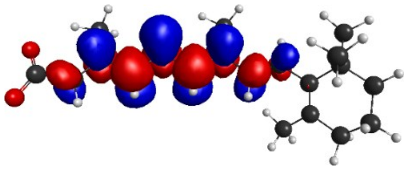	

SPISA spectroscopy – the effect of light fluence

The solution photoisomerisation action (SPISA) spectra in the paper were recorded using light fluences that gave no more than a few percent of photoisomerisation signal across the relevant photon energy range. Fig. S7(a) shows the yield of 13-*cis*, 9-*cis* and *multicis* photoisomers with relative light fluence at the photon energy of 3.49 eV (355 nm). Fig. S7(b) shows the 9-*cis*:13-*cis* photoisomer ratio and the *multicis*:13-*cis* photoisomer ratio with relative light fluence at the photon energy of 3.49 eV (355 nm). The *multicis*:13-*cis* photoisomer ratio approaches zero at low relative light fluence, confirming that *multicis* photoisomers are formed through sequential isomerisation processes. Note, the 13-*cis* signal probably includes a minor amount of 11-*cis*.

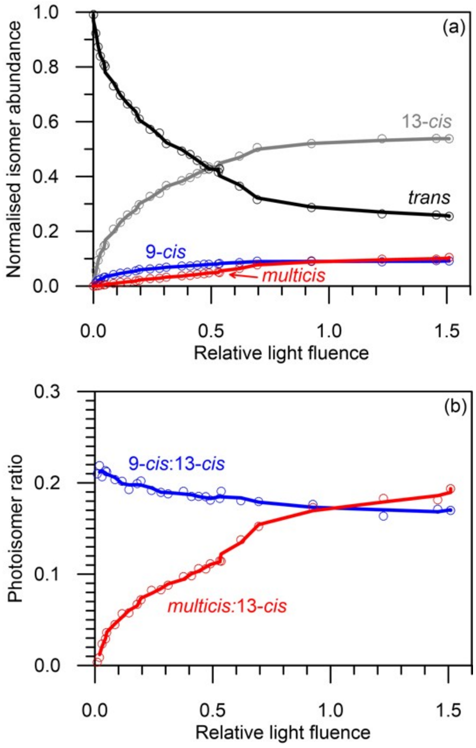

Fig. S7 – Photoisomer yields from *trans*-RA⁻ in pH > 11 methanol as a function of relative light fluence at the photon energy of 3.49 eV (355 nm): (a) normalised photoisomer yield, and (b) photoisomer branching ratios with relative light fluence.